Structural and Electronic Properties of the Layered LiNi 0.5 Mn 0.5 O 2 Lithium Battery Material

ARTICLE *in* CHEMISTRY OF MATERIALS · NOVEMBER 2003

Impact Factor: 8.35 · DOI: 10.1021/cm031098u

3 AUTHORS:

M. Saiful Islam
University of Bath
175 PUBLICATIONS **7,443** CITATIONS
SEE PROFILE

Richard Andrew Davies
Bangor University
19 PUBLICATIONS **509** CITATIONS
SEE PROFILE

Julian David Gale
Curtin University
270 PUBLICATIONS **14,958** CITATIONS
SEE PROFILE

Structural and Electronic Properties of the Layered $LiNi_{0.5}Mn_{0.5}O_2$ Lithium Battery Material

M. Saiful Islam,*,† R. Andrew Davies,† and Julian D. Gale‡

Department of Chemistry, University of Surrey, Guildford, GU2 7XH, U.K., and Department of Chemistry, Imperial College, London SW7 2AZ, U.K.

Received June 17, 2003. Revised Manuscript Received August 18, 2003

Computational studies based upon density functional theory (DFT) have been carried out on the $Li_xNi_{0.5}Mn_{0.5}O_2$ system, a promising cathode material for rechargeable lithium batteries. Electronic structure calculations suggest that the nominal valence state distribution is given by the formula $LiNi^{II}_{0.5}Mn^{IV}_{0.5}O_2$. Possible Ni−Mn cation ordering schemes in the layered structure have been examined including intralayer and interlayer configurations. The results on lithium deintercalation of $Li_xNi_{0.5}Mn_{0.5}O_2$ indicate that the electrochemical behavior is linked to the oxidation of Ni^{2+}. Our calculated cell voltage range as a function of lithium content (x) is compatible with electrochemical measurements that generally show sloping voltage profiles. The calculated Mn−O bond length shows relative invariance with Li extraction, whereas the Ni−O bond shortens significantly, which accords well with the available structural data.

1. Introduction

The study of new materials for rechargeable lithium batteries for applications in portable electronics is now a major field of materials research. Layered structured $LiCoO_2$ is the conventional and most commonly used cathode material, but poses problems associated with the high cost and toxicity of cobalt. Considerable attention has therefore been paid to other transition metal oxides as alternative cathode materials, especially oxides based on manganese such as layered $LiMnO_2$ and spinel-structured $LiMn_2O_4$.[1] However, various limitations with these systems have been found in comparison with $LiCoO_2$, which largely relate to capacity fading, phase instability, or structural transformation that occur with cycling.

In this context, there has been recent interest in mixed Li−Ni−Mn−O layered oxides,[2−9] particularly the $LiNi_{0.5}Mn_{0.5}O_2$ and T2-type $Li_{2/3}Ni_{1/3}Mn_{2/3}O_2$ phases, which show promising electrochemical and safety characteristics. Early work of Rossen et al.[2] investigated the solid-state synthesis and electrochemistry of the solid-solution $LiMnO_2$−$LiNiO_2$. Spahr et al.[4] prepared layered $LiNi_{1-y}Mn_yO_{2+\delta}$ ($0 \le y \le 0.5$) via an oxidative coprecipitation process, whereas Caurant et al.[3] used a soft chemistry ("chimie douce") route. For the $LiNi_{0.5}Mn_{0.5}O_2$ material, there has been some debate as to whether the mixed-metal oxide is comprised of either Ni^{2+}/Mn^{4+} (with cycling between Ni^{2+} and Ni^{4+}) or Ni^{3+}/Mn^{3+}. The XPS and magnetic measurements of Spahr[4] found strong enrichment of lithium at the surface and suggest that both Ni and Mn are in the +3 valence state within the bulk with Mn^{3+} being the electroactive species. Ohzuku and Makimura[5] presented recent work on the $LiNi_{0.5}Mn_{0.5}O_2$ system, showing a hexagonal structure, a sloping discharge profile, and a reversible capacity (ca. 150 mA h g^{-1}) in the voltage range 2.5−4.3 V. XANES studies of Yoon et al.[8a] conclude that the charge compensation when charging is achieved by the oxidation of Ni^{2+} to Ni^{4+}, but discharging at a low-voltage plateau is linked to reduction of Mn^{4+}. More recently, Kobayashi and co-workers[7] reported diffraction and X-ray absorption data for $Li_{1-x}Ni_{0.5}Mn_{0.5}O_2$, which show Ni^{2+}/Mn^{4+} valence states. Johnson et al.[8b] have also presented diffraction and XAS studies of $Li_xNi_{0.5}Mn_{0.5}O_2$, including the formation of the dilithium compound, $Li_2Ni_{0.5}Mn_{0.5}O_2$, with a hexagonal structure.

* To whom correspondence should be addressed. Tel: +44-1483-686844. Fax: +44-1483-686851. E-mail: m.islam@surrey.ac.uk.
† University of Surrey.
‡ Imperial College.

(1) (a) Bruce, P. G. *Chem. Commun.* **1997**, 1817. (b) Thackeray, M. M. *Prog. Solid State Chem.* **1997**, *25*, 1. (c) Whittingham, M. S.; Zavalij, P. Y. *Solid State Ionics* **2000**, *131*, 109. (d) Ammundsen, B.; Paulsen, J. *Adv. Mater.* **2001**, *13*, 943. (e) Amatucci, G.; Tarascon, J. M. *J. Electrochem. Soc.* **2002**, *149*, K31.

(2) Rossen, E.; Jones, C. D. W.; Dahn, J. R. *Solid State Ionics* **1992**, *57*, 311.

(3) Caurant, D.; Baffier, N.; Bianchi, V.; Grégoire G.; Bach, S. *J. Mater. Chem.* **1996**, *6*, 1149.

(4) Spahr, M. E.; Novák, P.; Schnyder, B.; Haas, O.; Nesper, R. *J. Electrochem. Soc.* **1998**, *145*, 1113.

(5) Ohzuku, T.; Makimura, Y. *Chem. Lett.* **2001**, 744.

(6) Lu, Z.; Beaulieu, L. Y.; Donaberger, R. A.; Thomas, C. L.; Dahn, J. R. *J. Electrochem. Soc.* **2002**, *149*, A778.

(7) (a) Kobayashi, H.; Sakaebe, H.; Kageyama, H.; Tatsumi, K.; Arachi, Y.; Kamiyama, T. *J. Mater. Chem.* **2003**, *13*, 590. (b) Arachi, Y.; Kobayashi, H.; Emura, S.; Nakata, Y.; Tanaka M.; Asai, T. *Chem. Lett.* **2003**, *32*, 60.

(8) (a) Yoon, W.-S.; Paik, Y.; Yang, X.-Q.; Balasubramanian, M.; McBreen, J.; Grey, C. P. *Electrochem. Solid-State Lett.* **2002**, *5*, A263. (b) Johnson, C. S.; Kim, J. S.; Kropf, A. J.; Kahaian, A. J.; Vaughey, J. T.; Fransson L. M. L.; Edstrom K.; Thackeray, M. M. *Chem. Mater.* **2003**, *15*, 2313.

(9) (a) Lu. Z.; Donaberger, R. A.; Dahn, J. R. *Chem. Mater.* **2000**, *12*, 3583. (b) Johnson, C. S.; Kim, J. S.; Kropf, A. J.; Kahaian, A. J.; Vaughey, J. T.; Thackeray, M. M. *Electrochem. Commun.* **2002**, *4*, 492 (c) Neudecker, B. J.; Zuhr, R. A.; Kwak B. S.; Bates, J. B.; Robertson, J. D. *J. Electrochem. Soc.* **1998**, *145*, 4148. (d) Quine, T. E.; Duncan, M. J.; Armstrong, A. R.; Robertson A. D.; Bruce, P. G. *J. Mater. Chem.* **2000**, *10*, 2838. (e) Shaju, K. M.; Rao, G. V. S.; Chowdari, B. V. R. *J. Electrochem. Soc.* **2003**, *150*, A1.

10.1021/cm031098u CCC: $25.00
Published on Web 10/09/2003

It is apparent in this research area of lithium battery materials that the underlying structural and electronic properties of transition metal oxides can be very complex, but are crucial to the complete understanding of the electrochemical behavior of cathode materials. The present study uses advanced computational techniques based on density functional theory (DFT) to investigate key issues of structure, lithium insertion, and valence states of the $LiNi_{0.5}Mn_{0.5}O_2$ system at the atomic and electronic level. Such computational techniques have been applied successfully to analogous studies of other oxide materials for lithium batteries.[10−13] Electronic and structural changes occurring during deintercalation are examined, including the calculation of average cell voltages as a function of lithium content.

2. Methodology

Recent developments have made computational techniques a powerful tool for the accurate prediction of the energetic, electronic, and structural aspects governing lithium intercalation into a wide range of transition metal oxides such as $Li_xV_2O_5$,[10] $Li_xMn_2O_4$-based spinels,[11] and layered Li_xMO_2.[12,13]

The present electronic structure calculations were performed within the framework of density functional theory (DFT) with the exchange-correlation energy being treated using the spin-polarized version of the generalized-gradient approximation (GGS-PW91).[14] Infinite lattice systems are modeled using periodic boundary conditions. The particular implementation of DFT used here combines a plane-wave basis set with the total energy pseudopotential method, as embodied in the CASTEP code,[15] which is ideally suited to calculations on periodic systems. This approach assumes that the tightly held core electrons are in the same states as in the free atoms, with the pseudopotential representing the interaction between valence electrons and the atomic cores via a nonlocal potential. Our present study complements recent related work of Reed and Ceder[13] using similar DFT methods, although direct quantitative comparison is difficult due to the need for further computational details (plane-wave cutoffs, *k*-point sampling schemes).

Our calculations on Li_xMO_2 (M = Ni, Mn) are based upon ultrasoft pseudopotentials of the form due to Vanderbilt,[16] with a plane-wave cutoff of 600 eV to ensure good convergence of the total energy differences and forces. Nonlinear core corrections were included for 3d elements, which typically leads to good agreement of spin-polarization and s−d transfer energies with all-electron calculations.[17] The reference atomic valence configurations used to construct the pseudopotentials are as follows: Li ($1s^22p^1$), O ($2s^22p^4$), Mn ($4s^23d^5$), and Ni ($4s^23d^8$). The Brillouin zone was sampled according to the Monkhorst-Pack scheme,[18] using a sufficiently large number of symmetry unique *k*-points for convergence of each system, namely, 90 and 16 *k*-points for supercells with formulas of Li_2NiMnO_4 and $Li_8Ni_4Mn_4O_{16}$, respectively. A coarser *k*-point sampling scheme was utilized for the larger supercells for computational efficiency due to the increased expense of the plane wave basis set as the volume is increased. Electronic relaxation was accomplished using a self-consistent density mixing scheme.[19] Geometry optimizations were performed using the BFGS algorithm to update an initial estimate of the Hessian, while also adopting a finite basis set correction to the total energy, which corrects for incompleteness of the plane wave basis set as the cell dimensions vary.[20]

All the present calculations are performed within the framework of nonlocal density functional theory, which has been applied successfully to numerous studies of oxide materials for lithium ion batteries.[10−13] However, we recognize that there are limitations in the accuracy of present gradient-corrected functionals, such as the self-interaction error and the systematic overestimation of cell volumes. Hence, we propose in future work to investigate the sensitivity of the present results on spin states to the introduction of Hartree−Fock exchange.

3. Results and Discussion

3.1. Structural and Electronic Simulation of $LiNi_{0.5}Mn_{0.5}O_2$. To probe the validity of our computational approach, structural optimizations of both $LiNiO_2$ and $LiNi_{0.5}Mn_{0.5}O_2$ were first performed based on the layered-hexagonal structures observed experimentally.[5,7,21−23] $LiNiO_2$ prepared by solid-state methods crystallizes with the α-$NaFeO_2$ O3-structure of $R\bar{3}m$ symmetry.[21−23] The structure can be described by $[MO_2]$ sheets consisting of edge-sharing MO_6 octahedra, with mobile lithium ions occupying octahedral sites between the $[MO_2]$ sheets.

Hexagonal $LiNiO_2$ was input using the conventional rhombohedral primitive unit cell and equilibrated under constant pressure conditions, allowing both the unit cell parameters and oxygen positions to vary. The calculated and experimental structural parameters are listed in Table 1 and show general accord to within 1% for the unit cell constants, the Ni−O bond length, and the interlayer distance. The electronic structure results reveal an energetic preference of 0.72 eV for the low-spin d^7 ($t_{2g}^6e_g^1$) Ni^{3+} configuration compared with the corresponding high-spin ($t_{2g}^5e_g^2$) state. This is in ac-

(10) Braithwaite, J. S.; Catlow, C. R. A.; Gale, J. D.; Harding, J. H. *Chem. Mater.* **1999**, *111*, 1990.
(11) (a) Braithwaite, J. S.; Catlow, C. R. A.; Harding, J. H.; Gale, J. D. *Phys. Chem. Chem. Phys.* **2000**, *2*, 3841. (b) Ammundsen, B.; Rozière, J.; Islam, M. S. *J. Phys. Chem. B* **1997**, *101*, 8156. (c) Ammundsen, B.; Burns, G. R.; Islam, M. S.; Kanoh, H.; Rozière, J. *J. Phys. Chem. B* **1999**, *103*, 5175. (d) Islam, M. S.; Ammundsen, B. In *Materials for Lithium-Ion Batteries*; Julien, C., Stoynov, C., Eds.; Kluwer Academic Publishers: The Netherlands, 2000; pp 293−307.
(12) (a) Aydinol, M. K.; Kohan, A. F.; Ceder, G.; Cho, K.; Joannopoulos, J. *Phys. Rev. B* **1997**, *56*, 1354. (b) Mishra, S. K.; Ceder, G. *Phys. Rev. B* **1999**, *59*, 6120. (c) Ceder, G.; Chiang, Y.-M.; Sadoway, D. R.; Aydinol, M. K.; Jang, Y.-I.; Huang, B. *Nature* **1998**, *392*, 694.
(13) Reed, J.; Ceder, G. *Electrochem. Solid-State Lett.* **2002**, *5*, A145.
(14) (a) Perdew, J. P.; Wang, Y. *Phys. Rev. B* **1992**, *46*, 6671. (b) White, J. A.; Bird, D. M. *Phys. Rev. B* **1994**, *50*, 4954.
(15) Payne, M. C.; Teter, M. P.; Allan, D. C.; Arias, T. A.; Joannopoulos, J. D. *Rev. Mod. Phys.* **1992**, *64*, 1045.
(16) Vanderbilt, D. *Phys. Rev. B* **1990**, *41*, 7892.
(17) Porezag, D.; Pederson M. R.; Liu, A. Y. *Phys. Rev. B* **1999**, *60*, 14132.
(18) Monkhorst, H. J.; Pack, J. D. *Phys. Rev. B* **1976**, *13*, 5188.
(19) (a) Kresse, G.; Furthmüller, J. *Phys. Rev. B* **1996**, *54*, 11169. (b) Bowler, D. R.; Gillan, M. J. *Chem. Phys. Lett.* **2000**, *325*, 473.
(20) Francis, G. P.; Payne, M. C. *J. Phys: Condens. Matter* **1990**, *2*, 4395.
(21) Arai, H.; Tsuda, M.; Sakurai, Y. *J. Power Sources* **2000**, *90*, 76.
(22) Barker, J.; Koksbang, R.; Saidi, M. Y. *Solid State Ionics* **1996**, *89*, 25.
(23) Hirano, A.; Kanno, R.; Kawamoto, Y.; Takeda, Y.; Yamaura, K.; Takano, M.; Ohyama, K.; Ohashi, M.; Yamaguchi, Y. *Solid State Ionics* **1995**, *78*, 123.

Table 1. Calculated and Experimental Structural Parameters of the Hexagonal ($R\bar{3}m$) O3-layered $LiNiO_2$ Unit Cell (Li^+ (3a) 0, 0, 0; Ni^{3+} (3b) 0, 0, $^1/_2$; O^{2-} (6c) 0, 0, *z*)

property	calculated	experiment[23]	Δ/%
$a = b$ (Å)	2.900	2.872	0.97
c (Å)	14.112	14.178	−0.47
volume (Å^3)	102.81	101.2	1.59
O(z)	0.2412	0.2413	−0.04
Ni−O (Å)	1.977	1.967	0.51
interlayer distance (Å)	4.704	4.726	−0.47

cordance with the observation of low-spin Ni^{3+} in $LiNiO_2$ from electron spin resonance and X-ray absorption spectroscopies.[24,25]

Our initial structural model for $LiNi_{0.5}Mn_{0.5}O_2$ is based upon the spin-polarized GGA optimized structure for isostructural $LiNiO_2$. Hexagonal superlattices of formula $Li_6Ni_3Mn_3O_{12}$ were generated from a $2 \times 1 \times 1$ periodic repeat of the optimized $LiNiO_2$ unit cell. Application of symmetry operations leads to three distinct supercells, two with formula $Li_6Ni_3Mn_3O_{12}$ and one with formula Li_2NiMnO_4 within the primitive cell. On energetic grounds, the monoclinic ($P12/m1$) supercell with formula Li_2NiMnO_4 is the most favorable ground-state configuration.

Electronic and structural optimization of $LiNi_{0.5}Mn_{0.5}O_2$ based on the Li_2NiMnO_4 supercell was performed under constant pressure conditions, allowing the unit cell parameters and ionic positions to relax. Dense *k*-point sampling consisting of 90 symmetry unique *k*-points ($6 \times 10 \times 6$ mesh) were employed to ensure convergence of energy differences and forces. A total of four different spin states related to the number of unpaired electrons were considered, each with different spin alignments corresponding to either Ni^{3+}/Mn^{3+} or Ni^{2+}/Mn^{4+}configurations. The relative energetics of $LiNi_{0.5}Mn_{0.5}O_2$ were investigated by fixing the number of unpaired electrons at these values, leading to four different configurations (labeled A, B, C, and D in Table 2). The calculated structural parameters of the hexagonal unit cell are also presented and compared with the experimental values in Table 2.

Examination of Table 2 indicates that configuration A related to Ni^{2+}/Mn^{4+} is the most energetically favorable and also possesses good structural accord with the experimental lattice parameters. In addition, the calculated metal−oxygen bond lengths for this configuration are consistent with those obtained from X-ray diffraction and EXAFS experiments.[7] In contrast, configuration B, C and D are higher in energy and some show considerable deviation from the observed crystal structure including a highly distorted NiO_6 octahedron. Moreover, initial geometry optimizations allowing the total number of unpaired electrons to vary at high *k*-point sampling also produced configuration A. We therefore focus on this configuration for the subsequent calculations in which the predicted valencies and spin states support the formation of Mn^{4+} and Ni^{2+}.

The electronic structure calculations therefore suggest that the nominal valence state distribution in the fully lithiated material is given by $LiNi^{II}_{0.5}Mn^{IV}_{0.5}O_2$ in which the extraction of lithium is predicted to involve oxidation of Ni^{2+}, a topic we return to below. This result is consistent with XANES measurements[7,8] and related DFT studies,[13] indicating that $LiNi_{0.5}Mn_{0.5}O_2$ contains Ni^{2+} and Mn^{4+}. In addition, the electrochemical behavior and ordering in $Li_{2/3}Ni_{1/3}Mn_{2/3}O_2$ has been rationalized by Lu et al.[9] in terms of a $Ni^{2+}-Mn^{4+}$ model rather than a $Ni^{3+}-Mn^{3+}$ model.

Table 2. Optimized Structures and Relative Energies of the Four Different Constrained Spin State Configurations for Hexagonal $LiNi_{0.5}Mn_{0.5}O_2$ (Experimental Structural Parameters Are Included for Comparison)

	spin state configuration				
property	(A)	(B)	(C)	(D)	expt[7]
number of unpaired electrons	1	3	5	7	
total |spin| density (a.u.)	4.40	3.32	5.20	7.09	
relative energy[a] (meV)	0	22	91	614	
a (Å)	2.930	2.954	2.926	2.959	2.892
c (Å)	14.206	14.134	14.409	14.538	14.301
volume (Å^3)	105.63	106.80	106.80	110.18	103.59
Ni−O (Å)	2.001 (×4) 2.124 (×2)	1.886 (×4) 2.526 (×2)	2.030 (×4) 2.102 (×2)	2.003 (×4) 2.132 (×2)	2.053, 2.07
Mn−O (Å)	1.974	1.971	1.988	1.983 (×4) 2.249 (×2)	1.990
interlayer distance (Å)	4.735	4.711	4.803	4.846	4.767

[a] Relative to configuration A (per formula unit).

We should note that direct comparison with experimental lattice parameters for $LiNi_{0.5}Mn_{0.5}O_2$ is not straightforward due to the possibility of some Ni in the Li layer.[7] This aspect has not been touched upon in certain structural reports. However, such Li/Ni mixing would result in differences in the observed cell parameters between various experimental studies due to the use of different synthesis conditions. This type of disorder could be related to the predicted electronic distribution comprised of Ni^{2+}, whereby this species would occupy the Li site, as found in $LiNiO_2$.[1] This is an obvious topic for further study.

While we have not sought to examine magnetic properties in detail, configuration A can be assigned to an antiferromagnetic arrangement of $Mn^{4+}(t_{2g}^3)$ and $Ni^{2+}(t_{2g}^6e_g^2)$, which is supported by our investigation of lithium deintercalation in section 3.3. With regard to our analysis, we have quoted the total spin density, which is a collective property of the whole system in that it has no dependence on the basis set. The integrated total spin density of 4.40 is slightly smaller than the minimum value of 5 electron spins expected for an antiferromagnetic arrangement of Mn^{4+} (3 unpaired electrons) and Ni^{2+} (2 unpaired electrons). Nevertheless, this result is in accordance with previous calculations,[13] where the net moment around both transition metal cations are lower than expected, with the remainder of the spin density on the oxygen sublattice; this could reflect the covalency in the material common to nickel oxides with Ni(3d)−O(2p) mixing. In this respect, Mack-

(24) Barra, A. L.; Chouteau, G.; Stepanov, A.; Delmas, C. *J. Magn. Magn. Mater.* **1998**, *177*, 783.

(25) (a) Rougier, A.; Delmas C.; Chadwick, A. V. *Solid State Commun.* **1995**, *94*, 123. (b) Nakai, I.; Takahashi, K.; Shiraishi, Y.; Nakagame, T.; Izumi, F.; Ishii, Y.; Nishikawa, F.; Konishi, T. *J. Power Sources* **1997**, *68*, 536.

rodt and co-workers[26] have used periodic Hartree−Fock methods to study transition metal monoxides and suggested, for example, that the hole state in Li-doped NiO is largely O(p).

3.2. Ni/Mn Cation Ordering. Superlattice cation ordering has been observed within lithium nickel−manganese oxides, such as P2-$Na_{2/3}Ni_{1/3}Mn_{2/3}O_2$ and T2-$Li_{2/3}Ni_{1/3}Mn_{2/3}O_2$,[6,9] in which the cations occupy prismatic and tetrahedral sites, respectively. $Li_{2/3}Ni_{1/3}Mn_{2/3}O2$ shows $Ni_{1/3}Mn_{2/3}$ honeycomb-type ordering in the transition metal layers. However, cation ordering has not been clearly characterized for O3-$LiNi_{0.5}Mn_{0.5}O_2$ from diffraction studies.[7,9]

To probe cation ordering within $LiNi_{0.5}Mn_{0.5}O_2$, a series of larger supercells with formula $Li_8Ni_4Mn_4O_{16}$ and *P*1 symmetry were created from $1 \times 2 \times 2$ periodic repeats of the optimized configuration A for Li_2NiMnO_4. Two main models of ordering of the Ni^{2+}/Mn^{4+} cations were explored: (a) interlayered ordering consisting of separate $\{NiO_6\}_\infty$ and $\{MnO_6\}_\infty$ layers (Figure 1a); and (b) intralayered ordering in which NiO_6 and MnO_6 octahedra alternate regularly within the same layer. The latter can be further divided into symmetric (Figure 1b) or antisymmetric (Figure 1c), depending upon the relative arrangement of the second layer with respect to the first layer. We note that given the size of the supercell that is presently feasible with first principles methods, it is impossible to create a cell large enough to have a truly random arrangement. The translational symmetry means that any attempt to make a random choice of positions is going to lead to an ordered structure. It is clear that the cations must be in equal numbers in each layer since the results demonstrate that the elastic energy penalty is too large to accommodate alternative configurations, which has allowed us to exclude some unstable models.

The energetics of the ordered supercells were investigated by performing a series of geometry optimizations with fixed numbers of electron spins. Preliminary calculations performed on the intralayered symmetric $LiNi_{0.5}Mn_{0.5}O_2$ show an energetic preference for a system with a zero net moment. This picture is consistent with the study of spin ordering in spinel-structured $Li_xCo_yMn_{4-y}O_8$ in which the electron spins order in an antiparallel manner so that the total number of unpaired electrons within the simulation cells are minimized.[11] This also agrees with the observation of Curie−Weiss behavior for $LiNi_{1-y}Mn_yO_2$ between 150 and 200 K, with negative paramagnetic Curie temperatures, indicative of antiferromagnetic interactions of the magnetic centers.[4] Magnetic hysteresis attributed to ferromagnetic interactions from the linear Ni^{2+}(3a)−O−Mn^{4+}(3b)−O−Ni^{2+}(3a) superexchange interaction has recently been observed within cation disordered $LiNi_{0.5}Mn_{0.5}O_2$.[7]

Our results in Table 3 indicate that the lowest energy ordering scheme is the intralayered symmetric arrangement in which NiO_6 and MnO_6 octahedra alternate within the same layer (Figure 1). This distribution will minimize the repulsive interactions between the mixed metal ions. The higher energy of the interlayered structure can be rationalized in terms of the excess strain energy between the two layers due to the marked difference between the smaller Mn^{4+} (0.53 Å) and the larger Ni^{2+} (0.69 Å). Due to the nature of the cell and

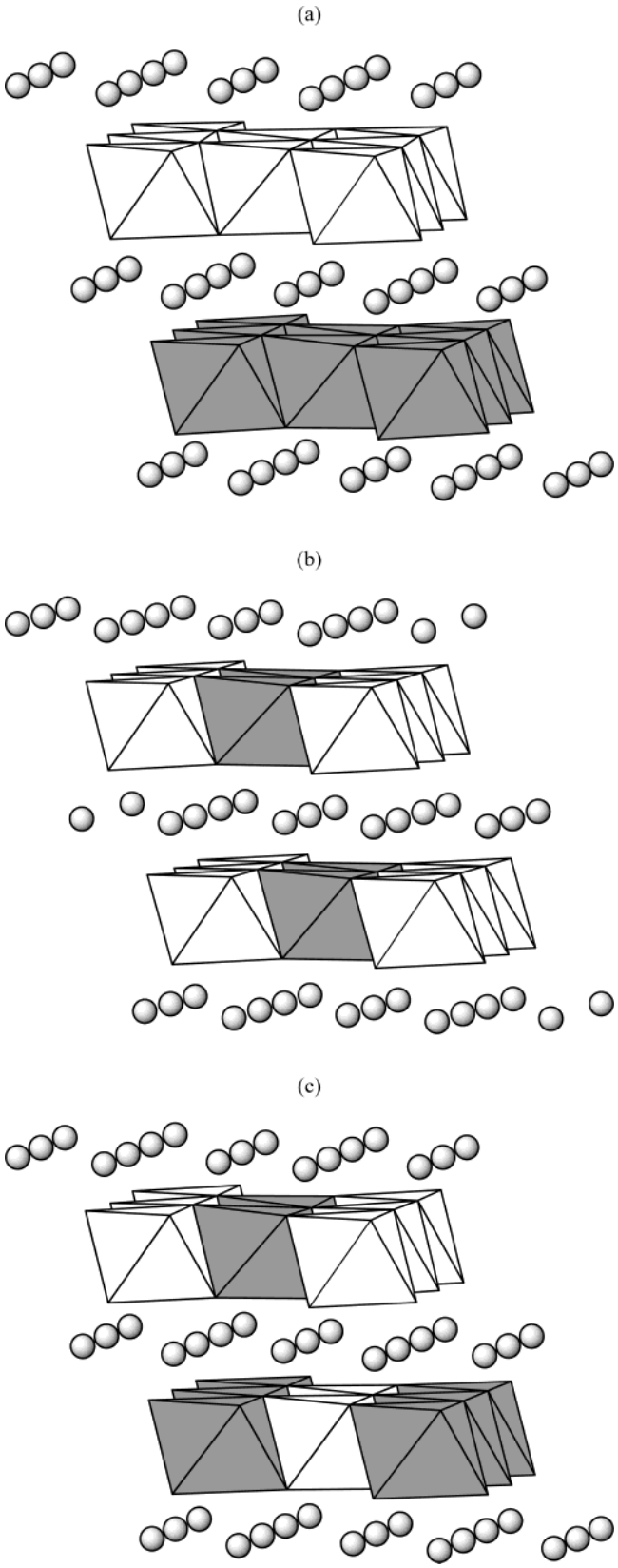

Figure 1. Cation ordering schemes within $LiNi_{0.5}Mn_{0.5}O_2$: (a) interlayer, (b) symmetric intralayer, (c) antisymmetric intralayer. (Ni^{2+} and Mn^{4+} cations are located within the unshaded and shaded octahedra, respectively.)

(26) (a) Mackrodt, W. C.; Harrison, N. M.; Saunders, V. R.; Allan, N. L.; Towler, M. D. *Chem. Phys. Lett.* **1996**, *250*, 66. (b) Mackrodt, W. C.; Noguera, C. *Surf. Sci.* **2000**, *457*, L386.

Table 3. Calculated Relative Energies for Cation Ordering Schemes of $LiNi_{0.5}Mn_{0.5}O_2$ (Based upon Monoclinic $Li_8Ni_4Mn_4O_{16}$ Supercells)

ordering scheme	relative energy[a] (meV)
intra-symmetric	0
intra-antisymmetric	255
interlayered	280

[a] Relative to intra-symmetric supercell.

the dominance of the elastic interaction for mixing Mn/Ni in the same layer, the Mn/Ni ions are forced to alternate to maximize the distances between the tetravalent ions. As for the spin states, the exchange interaction within the layers is much stronger than that between the layers as expected.

The energy differences between alternative cation arrangements suggests that, at least at low temperatures, configurational entropy terms are unlikely to be significant enough to generate a random distribution, and thus cation ordering could occur. It is worth noting that ordering of cations in the layer has been observed in $Li_{0.5}Ni_{0.5}Mn_{0.5}O_2$.[7] The T2-$Li_{2/3}Ni_{1/3}Mn_{2/3}O_2$ phase also shows in-plane superlattice ordering of Ni and Mn that is preserved during ion exchange.[9] We recognize, however, that further structural work is necessary to elucidate the possibility of Ni/Mn ordering in $LiNi_{0.5}Mn_{0.5}O_2$, which has not been clearly observed. At the high temperatures (>700 °C) used for materials' synthesis of this system, a random distribution may occur that would be retained on rapid cooling.

Using the lowest energy structure of $LiNi_{0.5}Mn_{0.5}O_2$, we then examined the degree of Ni−Mn interaction with respect to the component $LiMO_2$ oxides. This can be estimated by comparing the energy of the mixed oxide with the total mean energy of $LiNiO_2$ and $LiMnO_2$. We find that the energy of the $LiNi_{0.5}Mn_{0.5}O_2$ mixed system is negative (−147 meV) relative to the component oxides. This suggests that, at least at low temperatures, the $LiNi_{0.5}Mn_{0.5}O_2$ material (comprised of Ni^{2+} and Mn^{4+}) is favored over separate regions of $LiNi^{III}O_2$ and $LiMn^{III}O_2$.

3.3. Cell Voltages and Electronic Structure in $Li_xNi_{0.5}Mn_{0.5}O_2$. Previous studies performed on a wide variety of Li-intercalated transition metal oxides[10,12] have indicated that the average cell voltage can be derived using the Nernst relationship. For our system, lithium intercalation can be represented by the reaction

$$Li_{x_1}Ni_{0.5}Mn_{0.5}O_2 + (x_2 - x_1)\,Li = Li_{x_2}Ni_{0.5}Mn_{0.5}O_2 \quad (1)$$

where the free energy change (ΔG) can be approximated by the internal energy change per intercalated Li^+ (ΔE) since the vibrational and configurational entropy contributions to the cell voltage at room temperature are expected to be small as discussed by Catlow[10] and Ceder.[12] To estimate the internal energy, the energy $E(x)$ for a limited number of $Li_xNi_{0.5}Mn_{0.5}O_2$ phases are calculated together with the energy of lithium metal, E(Li). The change in total energy of the system per intercalated lithium atom is given by

$$\Delta E(\bar{x}) = \{E(x_2) - [E(x_1) + (x_2 - x_1)E(\mathrm{Li})]\}/(x_2 - x_1) \quad (2)$$

where $E(x)$ = total energy of $Li_xNi_{0.5}Mn_{0.5}O_2$, $x_2 > x_1$, and $\bar{x} = (x_1 + x_2)/2$. It is stressed that $\Delta E(\bar{x})$ leads to a predicted cell voltage that is an average value for all $Li_xNi_{0.5}Mn_{0.5}O_2$ compositions between x_1 and x_2. Very small changes in composition are required to calculate ΔE accurately, but this requires the construction of extremely large supercells at considerable computational expense. Nevertheless, our main task here is to derive reliable trends as a function of lithium content for which these methods are well-suited.

Table 4. Calculated Average Cell Voltages for $Li_xNi_{0.5}Mn_{0.5}O_2$ as a Function of Lithium Content (Voltages Are Calculated for an Average Composition between the Simulated Limits)

Li content, x	average cell voltage/V
0.75	3.00
0.50	3.32
0.25	3.64

The energy of lithium metal, E(Li), as the anode was obtained by optimization of body-centered cubic ($Im\bar{3}m$) Li metal with $a_0 = 3.491$ Å,[27] using 455 symmetry unique k-points based on a 25 × 25 × 25 Monkhorst-Pack mesh. Our initial studies used the smaller Li_2NiMnO_4 cells to derive average cell voltages for $x = 0.25$, 0.50, and 0.75.

The resulting data in Table 4 show a calculated voltage range of about 3.0−3.6 V for high to low lithium content (x), which is compatible with measured profiles. Electrochemical studies generally show sloping voltage profiles for $Li_xNi_{0.5}Mn_{0.5}O_2$ with cell voltage ranges of 3.6−3.9 V for high x (>0.75) and 4.0−4.3 V for low x (<0.5).[3−7] As with previous DFT-based studies, the quantitative discrepancy is consistent with the systematic underprediction of the cell potential in transition metal oxides of about 0.5−0.7 V.[10,12,13] We recognize that the dominant source of error is likely to be attributed to the overbinding of lithium metal. In any case, our calculated trend in cell voltages as a function of Li content is in accordance with measurements.

Our primary interest here was to probe the affect of lithium deintercalation on the electronic structure of $Li_xNi_{0.5}Mn_{0.5}O_2$. The charging process in such oxides is associated with electrochemical Li extraction linked to the oxidation of transition metal ions. The crystal structures considered contain two crystallographically distinct Li environments: neighboring either Mn^{4+}(0.5, 0.5, 0) or Ni^{2+}(0, 0, 0). The initial deintercalation process leads to the formation of monoclinic $Li_{0.5}Ni_{0.5}Mn_{0.5}O_2$ with a small energetic preference of 79 meV for the extraction of lithium ions nearest to the manganese ions.

Changes in the electronic structure of the layered host as lithium deintercalation takes place can be examined by subtracting electron (spin) density contributions of two phases with different lithium concentrations. This generates a difference density that indicates the regions that show significant change during the intercalation reaction. The resulting contour plots for $Li_{0.5}Ni_{0.5}Mn_{0.5}O_2$ and $Ni_{0.5}Mn_{0.5}O_2$ relative to $LiNi_{0.5}Mn_{0.5}O_2$ are shown in Figure 2. These results indicate that the dominant effect (ca. 85%) of lithium extraction from $Li_xNi_{0.5}Mn_{0.5}O_2$ is located on Ni. This is consistent with the loss of electron spin upon oxidation of Ni^{2+} ($t_{2g}^6e_g^2$) to

(27) Barrett, C. S. *J. Phys. Chem.* **1958**, *62*, 732.

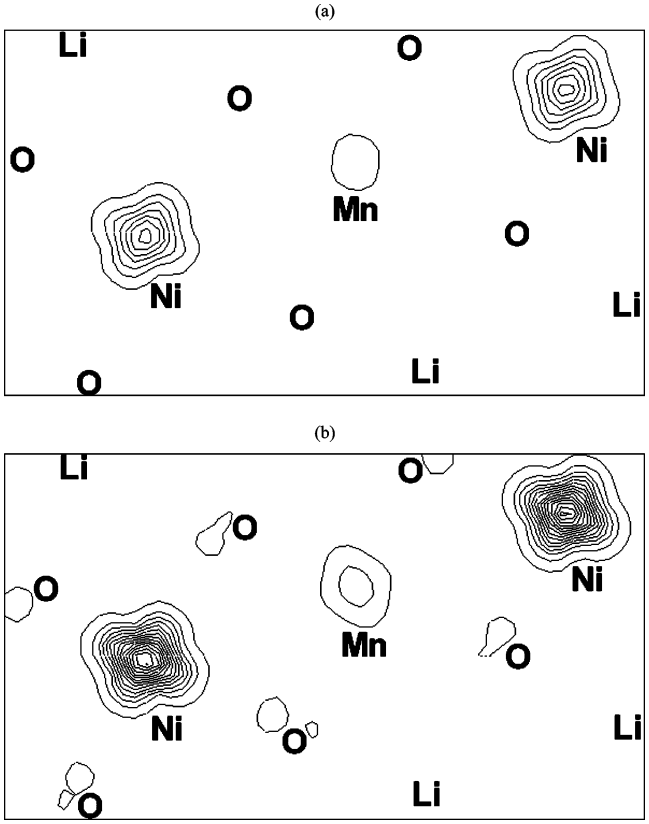

Figure 2. Electon spin density difference after lithium extraction from $Li_xNi_{0.5}Mn_{0.5}O_2$ relative to $x = 1$ (within the Ni−O−Mn plane). Contour lines indicate largest change: (a) $\rho(Li_{0.5}Ni_{0.5}Mn_{0.5}O_2) - \rho(LiNi_{0.5}Mn_{0.5}O_2)$, (b) $\rho(Ni_{0.5}Mn_{0.5}O_2) - \rho(LiNi_{0.5}Mn_{0.5}O_2)$.

Table 5. Calculated Cell Volumes and Mean Bond Lengths as a Function of Lithium Content (*x*) on Deintercalation of Monoclinic $Li_xNi_{0.5}Mn_{0.5}O_2$ (Available Experimental Bond Lengths[7] Are in Brackets)

	$Li_xNi_{0.5}Mn_{0.5}O_2$		
property	$x = 1$	$x = 0.5$	$x = 0$
volume (Å^3)	70.40	70.10	68.18
Ni−O (Å)	2.042 (2.053, 2.07)	1.931 (1.958)	1.904
Mn−O (Å)	1.974 (1.990)	1.973	1.948

low-spin Ni^{3+} ($t_{2g}^6e_g^1$) and low-spin Ni^{4+} (t_{2g}^6) and confirms that Ni is the redox-active species. However, there is a small change in electron spin density on the Mn (ca. 10%) and oxygen (ca. 5%) sublattices during lithium extraction, which reflects the covalent mixing in the system. We speculate that Mn is not completely inert and that the involvement of Mn, in the presence of Ni, may lead to higher cell voltages for the mixed metal cathode. The site energy for Li^+ will also be influenced by the mixed Ni−Mn lattice relative to $LiMO_2$. It is worth noting that $Li_xNi_{0.5}Mn_{0.5}O_2$ compositions containing mixed-valent Ni^{2+}/Ni^{3+} (or Ni^{3+}/Ni^{4+}) may exhibit electron transport associated with small polaron hopping, as found in other transition metal oxides.[1]

Analysis of the calculated bond lengths (Table 5) indicates that the Mn−O bond length shows little variation with Li composition, confirming the negligible change in Mn valence state. In contrast, the average Ni−O bond length changes significantly with Li content, from 2.04 Å for $LiNi_{0.5}Mn_{0.5}O_2$ to 1.93 Å for $Li_{0.5}Ni_{0.5}Mn_{0.5}O_2$. This result agrees well with the shortening in the mean Ni−O bond length from 2.053 to 1.958 Å observed from Ni−K edge EXAFS data for $Li_xNi_{0.5}Mn_{0.5}O_2$.[7] This decrease is again consistent with the oxidation of Ni^{2+} to the smaller ions, Ni^{3+} and Ni^{4+}. Recent XANES data[7,8] also indicate the oxidation of Ni^{2+} during charging with no observed chemical shifts in the Mn−K edge.

Table 6. Calculated and Experimental Structural Parameters for Monoclinic $Li_{0.5}Ni_{0.5}Mn_{0.5}O_2$

property	calculated	experimental[7]
a (Å)	5.014	4.924
b (Å)	2.891	2.852
c (Å)	5.052	5.087
β (deg)	106.79	108.81

The structural data in Table 5 reveal that the observed decrease in cell volume as the lithium content decreases is reproduced by the calculations. In this case, the variation in unit cell size is relatively smaller than that observed for $LiMn_2O_4$ spinel and may be related to the cycling stability of $Li_xNi_{0.5}Mn_{0.5}O_2$. It has also been suggested[8] that the relative stability of this layered system during cycling with respect to possible transformation to spinel is partly due to the absence of Mn^{3+}.

Finally, we find that our predicted monoclinic structure and unit cell parameters for $Li_{0.5}Mn_{0.5}Ni_{0.5}O_2$, in which we consider lithium ordering in the layer, are in good accord with X-ray diffraction data[7] refined with a monoclinic lattice (Table 6). Similar monoclinic structures have been observed for $Li_{1-x}NiO_2$ ($0.25 \leq x \leq 0.55$)[23,28] and $NaNiO_2$.[29] We recognize that the structural chemistry of layered $LiMO_2$ compounds is complex and suggest the need for further characterization studies of $Li_xNi_{0.5}Mn_{0.5}O_2$ across the Li composition range to fully optimize this system.

Conclusions

Computational studies based on DFT methods have assisted in advancing our understanding of the structural and electronic properties of the complex $Li_xNi_{0.5}Mn_{0.5}O_2$ lithium battery material, which complement related experimental and theoretical work. The following main points emerge from our study.

(1) Electronic structure calculations suggest that the nominal valence state distribution in the fully lithiated material is given by $LiNi^{II}_{0.5}Mn^{IV}_{0.5}O_2$. Cation ordering schemes of Ni^{2+}/Mn^{4+} were explored with the lowest energy predicted for the intralayered symmetric arrangement with alternating NiO_6 and MnO_6 octahedra, which minimizes the repulsive ion−ion interactions. Cation ordering in the layer has been observed in the $Li_{0.5}Ni_{0.5}Mn_{0.5}O_2$[7] and T2- $Li_{2/3}Ni_{1/3}Mn_{2/3}O_2$ [9] phases, although further structural work is necessary to elucidate the possibility of Ni/Mn ordering in $LiNi_{0.5}Mn_{0.5}O_2$.

(2) Our calculated cell voltage range as a function of lithium content (*x*) is compatible with electrochemical measurements on $Li_xNi_{0.5}Mn_{0.5}O_2$, which generally show sloping voltage profiles. The dominant effect of lithium deintercalation is localized on Ni; this suggests that Ni is the redox-active species, cycling between Ni^{2+} and

(28) Ohzuku, T.; Ueda, A.; Nagayama, M. *J. Electrochem. Soc.* **1993**, *140*, 1862.
(29) Dyer, L. D.; Borie, B. S., Jr.; Smith, G. P. *J. Am. Chem. Soc.* **1954**, *76*, 1449.

Ni^{4+} within a stable manganese−oxygen matrix. However, there is a small change in electron spin density on the Mn and oxygen sublattices during lithium extraction, which reflects the covalent mixing in the system. We speculate that the involvement of Mn, in the presence of Ni, may lead to slightly higher cell voltages within the mixed-metal oxide. It is worth noting that compositions containing mixed-valence Ni^{2+}/Ni^{3+} (or Ni^{3+}/Ni^{4+}) may exhibit electron transport associated with small polaron hopping, as found in other transition metal oxides.

(3) The calculated Mn−O bond length shows relative invariance with Li extraction, whereas the mean Ni−O bond length shortens significantly from 2.04 Å for $LiNi_{0.5}Mn_{0.5}O_2$ to 1.93 Å for $Li_{0.5}Ni_{0.5}Mn_{0.5}O_2$. This is consistent with the oxidation of Ni^{2+} to the smaller Ni^{3+}. Our predicted monoclinic structure for $Li_{0.5}Mn_{0.5}Ni_{0.5}O_2$, in which we consider lithium-vacancy ordering in the layer, is in accordance with the available diffraction data.

We recognize, however, the possibility of a small amount of Ni on the Li sites in $LiNi_{0.5}Mn_{0.5}O_2$, which has not been fully addressed by some structural studies. Our future computational work will include defect simulations on cation disordering between Li and Ni−Mn layers, as well as further examination of the influence of density functional exchange versus Hartree−Fock exchange with regard to the spin state preference.

Acknowledgment. We wish to acknowledge the EPSRC, the Materials Chemistry Consortium for Cray T3E time, and the JREI for Compaq resources at RAL. We are also grateful to Dr. Brett Ammundsen (Pacific Lithium, NZ) and Dr. Furio Corá (The Royal Institution, UK) for useful discussions.

CM031098U